Mixed model for the analytical determination of critical buckling load of passive reinforcement in compressed RC and FRC elements under monotonic loading

Javier Pereiro-Barceló, José L. Bonet*

Instituto de Ciencia y Tecnología del Hormigón, ICITECH, Universitat Politècnica de València, Camino de Vera s/n, 46022 Valencia, Spain

ABSTRACT

Compressed reinforcements on reinforced concrete (RC) and steel fibre reinforced concrete (SFRC) columns are generally submitted to cyclic and monotonic loading, which can buckle. This phenomenon can cause the reduction of both ductility and peak loads, which is why design standards propose constructive details to avoid this. Although the bibliography mentions that steel fibres in concrete can delay buckling of reinforcements, design codes do not distinguish between concrete types (with and without fibres) in these constructive details. Analytical models that determine the length and critical buckling stress of reinforcements may consider this effect. Nowadays, analytical models can be classified as discrete and distributed depending on whether they consider transverse reinforcement stiffness and the stiffness of the concrete cover that concentrates on transverse reinforcements, or if they are distributed along the element, respectively. Both discrete and distributed models are valid for small transverse reinforcement separations, while distributed models that only consider the concrete cover effect are valid for large transverse reinforcement separations.

This paper proposes a mixed model to determine critical buckling loads of compressed reinforcements subjected to monotonic loading to use the stress-strain relationships of reinforcing bars, including buckling, that are found in the scientific-technical literature. This model considers transverse reinforcements discretely and concrete cover distributedly. The model can be applied to any transverse reinforcement configuration, and to any concrete type (with or without fibres). An analytical equation is also proposed to determine critical compressed reinforcement loads, whose result is presented as abaci. Finally, to calibrate the model in normal-strength concrete columns under eccentric loading, with or without fibres, a programme is presented in which the critical load of longitudinal reinforcements is experimentally determined. The proposed analytical model is calibrated and a procedure to determine critical buckling loads of compressed reinforcements under monotonic loading is proposed.

© 2017.

1. Introduction

Longitudinal reinforcements can buckle in columns subject to monotonic and cyclic loading on reinforced concrete (RC) and steel fibre reinforced concrete (SFRC) elements. This effect drastically reduces the expected ductility. This may be due to an insufficient quantity of or incorrectly arranged transverse reinforcement, or to the concrete cover degrading. In order to avoid reinforcements from buckling, structure codes (EHE-08 [1], EN 1998-1:2004 [2], EN 1998-2:2005 [3], ACI 318-14 [4]) propose relations between the diameters of transverse and longitudinal reinforcements, and the maximum separations of transverse reinforcements. However, these codes do not bear in mind the favourable effect of steel fibres (Caballero et al. [5], Caballero et al. [6], Paultre et al. [7]). This effect can be considered in analytical models to determine the load and critical length of buckling.

Nowadays, analytical models are classified as discrete and distributed (Table 1) depending on how they consider the transverse reinforcement and/or concrete cover. The models that only consider transverse reinforcements discretely (Papia et al. [8] and Dhakal and Maekawa [9]) generally obtain a lower critical load rate. Discrete and distributed models are valid for small transverse reinforcement separations, and only distributed models that consider concrete cover are valid for large separations. Consequently, no analytical model is valid for intermediate separations.

It is worth indicating that only the models of Dhakal [10] and Campione [11] have contemplated the contribution of steel fibres to concrete covers. Concrete with fibres confers greater ductility to elements as the strain at peak stress increases considerably, and the softening branch delays cover spalling. Therefore, their use improves how the element behaves under cyclic loading. Nonetheless, Dhakal [10] does not consider the progressive loss of concrete cover stiffness, which results in overestimating buckling stress.

Table 1
Authors who have studied local compressed passive reinforcement buckling.

Authors	What the model considers				Concrete with fibres
	Transverse reinforcement		Concrete cover		
	Discrete	Distributed	Discrete	Distributed	
Bresler and Gilbert [18]		x			No
Scribner [19]		x			No
Pantazopoulou [32]		x			No
Dhakal and Maekawa [9]	x				No
Dhakal [10]	x		x		Yes
Campione [11]		x		x	Yes
Taalat [21]		x			No
Papia et al. [8]	x				No

Several researchers have carried out experimental tests on compressed passive reinforcement buckling. Of all these tests, the only ones that provide data about buckling bar stresses and strains are tests on isolated bars (Mander [12], Mander [13], Monti and Nuti [14], Rodriguez et al. [15], Bayrak and Sheikh [16], Bae et al. [17]). Other authors have analysed local reinforcement buckling on reinforced concrete elements (Bresler and Gilbert [18], Scribner [19]) did not directly measure buckling strain on bars. During these tests, the critical buckling stress or strain was obtained by indirect methods, and/or observations were made about how many transverse reinforcements were involved when the tests ended.

The scientific literature shows there are no analytical models available that assess compressed reinforcement buckling that consider: transverse reinforcements discretely, concrete cover (with/without fibres) distributedly and for any transverse reinforcement separation. Since no experimental tests have been done that offer critical buckling stresses or strains of passive longitudinal reinforcements inserted into a concrete section, it is necessary to undertake an experimental campaign for this purpose using concretes with and without fibres in order to calibrate the analytical model proposed herein.

2. Research significance

The objective of this paper is to propose a mixed analytical model to determine the critical buckling load of compressed reinforcements in RC and SFRC elements, subject to monotonic loading for any transverse reinforcement distribution and separation, and for reinforced concrete elements either with or without fibres. This model considers transverse reinforcements discretely and concrete covers distributedly. As a result of applying the model, an analytical equation is proposed to calculate critical buckling loads. The results of the model are also shown as abaci. As there is a gap of experimental results to determine critical buckling loads on compressed bars, an experimental programme with NSC columns (with/without fibres) is proposed to calibrate the proposed analytical model. A procedure is proposed to determine critical buckling loads by taking the proposed mixed analytical model as a reference.

3. Proposed analytical model

To determine the critical load, the bifurcation approach is used (Chen and Lui [20]). An equilibrium equation at the deflected shape is formulated by the classical column theory. The assumptions made

are:

1. The column is perfectly straight
2. The axial load is applied along the centroidal axis of the column
3. Plane sections before applying strain remained plane after applying strain
4. Member deflection is due only to bending
5. The material obeys Hooke's Law (stress and strain are linearly related)
6. Member deflection is small. As a result, the curvature can be approached by the second derivative of lateral displacement

The proposed model is based on Papia et al. [8]. It considers transverse reinforcements discretely and is extended so that it contemplates the concrete cover distributedly.

3.1. General model description

Fig. 1 shows the forces that act on a bar at its deflected shape along the length of the region that involves instability L. These forces are: discrete forces caused by transverse reinforcement (F_i); distributed force due to concrete reinforcement (F_c); axial bar force (P); bending moment on ends (M_0).

If the number of transverse reinforcements along length L is even, segments j will fall between 0 and 2n (Fig. 1(a)). If the number of transverse reinforcements is odd, segments j will fall between 0 and $2n - 1$ (Fig. 1(b)). The separation between transverse reinforcements is s. The y-z axes are the global bar axes, while x is the local axis of each segment j. The forces generated by both transverse reinforcement (F_i) and concrete cover (F_c), depend on the deflected shape of buckled compressed bar. Transverse reinforcement can be represented as intermediate unilateral elastic supports, whose stiffness is α_s. Consequently, force F_i is obtained as a product of stiffness α_s by the displacement on elastic support $y_j(x = 0)$. The number of supports n_0 in the instability zone is 2n if the number of transverse reinforcements is even, and $2n - 1$ if it is odd. The cover is modelled as an element with distributed stiffness (α_c) along length L. It was hypothesised that the stiffness of the transverse reinforcements was equal for them all, and that the distributed stiffness of the cover was constant along length L.

3.2. Analytical consideration

For each segment j the equilibrium equation at the deflected shape is:

$$E_r \cdot I \cdot \frac{d^2 y_j(x)}{dx^2} = -(P \cdot y_j(x) - M_0 - Ms_j(x) - Mc_j(x)) \tag{1}$$

where:

E_r: the reduced elasticity module of the longitudinal reinforcement (Fig. 2) on the circular section proposed by Papia et al. [8]

$$E_r = E_s \cdot \frac{4}{\pi} \cdot \left[\varphi(\theta_0) + \varphi(\pi - \theta_0) \frac{E_h}{E_s} \right] \tag{2}$$

where:

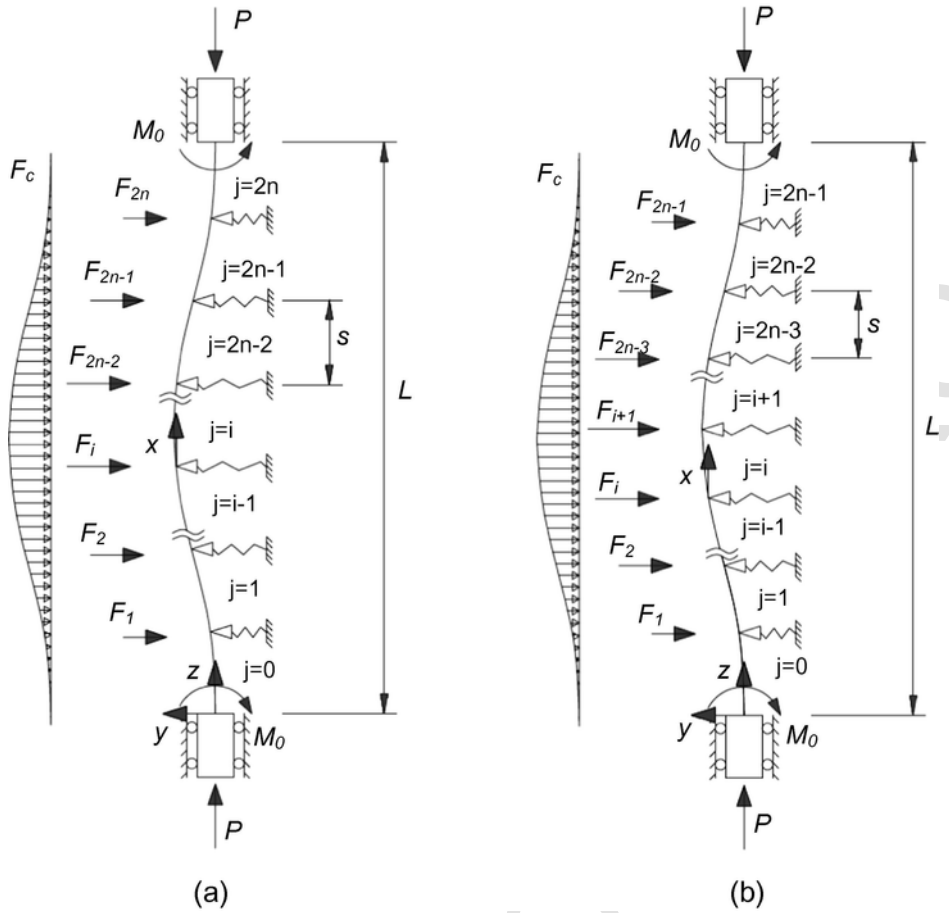E_s: the compressed elasticity module

Fig. 1. Analysis model: (a) Even number of transverse reinforcements: j between 0 and 2n, (b) Odd number of transverse reinforcements: j between 0 and 2n − 1.
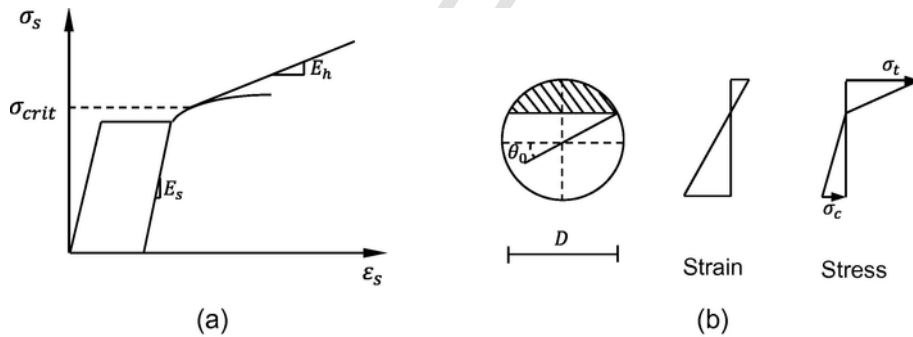

Fig. 2. The instability situation of reinforcing bars: (a) The stress- strain diagram, (b) The diagram illustrating the stresses and strains of the cross section of the compressed bar.

E_h: the tangent module of the plastic branch in the compressed stress-strain diagram

θ_0: the neutral fibre position on the polar coordinates obtained from the following implicit equation:

$$\frac{E_h}{E_s} = \frac{\sin\theta_0 - 1/3\sin^3\theta_0 - \theta_0\cos\theta_0}{\sin\theta_0 - 1/3\sin^3\theta_0 + (\pi - \theta_0)\cos\theta_0} \tag{3}$$

$\varphi(\theta_0)$: the shape function to determine E_r on the circular sections to position the neutral fibre θ_0.

$$\varphi(\theta_0) = 1/4\left[\theta_0 - \left(\frac{5}{2} - 1/3\sin^2\theta_0\right)\sin 2\theta_0 \right.$$
$$\left. + 4\theta_0\cos^2\theta_0\right] \tag{4}$$

$y_j(x)$: coordinates of displacement "y" of segment j according to x

P: axial force applied to bar ends

I: inertia moment of the longitudinal bar

M_0: bending moment of the built-in bar ends in the region that involves instability

$Ms_j(x)$: bending moment due to the lateral loads generated by the transverse reinforcement at any point x of a segment j

$Mc_j(x)$: bending moment due to the lateral loads generated by the concrete cover at any point x of a segment j

Eq. (1) is a second-order differential equation with constant coefficients. As the problem presents symmetry (Fig. 3), deflected shape $y_j(x)$ of each segment j is obtained from solving a system with n + 1 differential equations if number n_0 is even and with n differential equations if n_0 is odd. The equation of $Ms_j(x)$ according to Fig. 3 is as follows:

$$Ms_j(x) = (1 - \delta_j^n) \cdot z(j,x) \cdot \left(\sum_{i=j+1}^{n} (F_i) - qF_n \right)$$
$$+ (1 - \delta_j^0) \cdot (\mu s F_1) + \left(\sum_{i=2}^{j} (\mu l + (i-1)s) \right) F_i \quad (5)$$

where:

$\delta_b' a$: Kronecker delta whose value is 1 if a = b and 0 if a ≠ b

q: it is 0 if n_0 is even and 0.5 if n_0 is odd

μ: factor between 0 and 1.

$z(x,j)$: global coordinates of position x on local axes in a segment j:

$$z(j,x) = (x + (1 - \delta_j^0)s \cdot (\mu + (j-1))) \quad (6)$$

To obtain the equation of $Mc_j(x)$, it is assumed that the lateral force caused by the concrete cover distributed along length L is cubic-shaped $g(z)$. This implies that the deflected shape can also be cubic-shaped. This hypothesis is justified by:

– The deflected shape caused by discrete loads (transverse reinforcement) on a fixed-fixed column is a third-degree polynomial

– According to Taalat [21] and Campione [11], the deflected shape of the bar comes as $\sum_{r=1}^{\infty} \delta/2(1 - \cos(2\pi rx/L))$ where δ is the maximum bar displacement by only assuming a distributed lateral force due to the concrete cover and/or transverse reinforcement. In the buckling case, r equalled 1 and this equation can be quite accurately approached to a third-degree polynomial.

– Bearing in mind the two previous sections, that material behaviour is linear, transverse reinforcement is modelled as discrete loads and the concrete cover is modelled as a distributed load, the deflected shape that causes both load distributions will be cubic.

The contour conditions of function $g(z)$ are:

$$g(z = 0) = 0; g(z_n)$$
$$= F_n/\alpha_s; g'(z$$
$$= 0)$$
$$= 0; g'(z$$
$$= L/2)$$
$$= 0 \quad (7)$$

where:

z_n: coordinate z of force F_n equals $\mu s + (n - 0.5)s$ if n_0 is even and equals $L/2$ if n_0 is odd.

Consequently, the equation of $Mc_j(x)$ at point x of a segment j is obtained from the following equation:

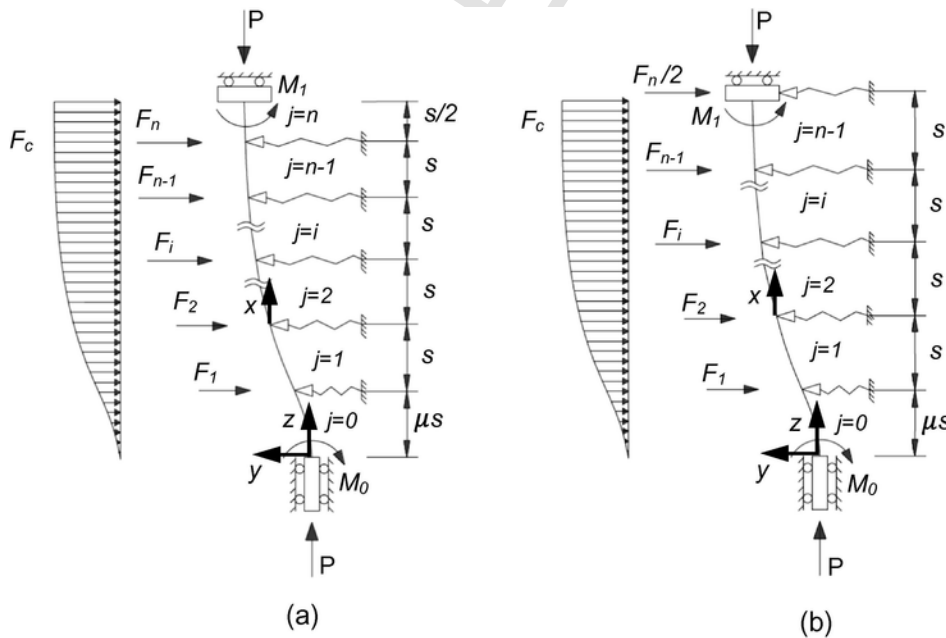$$Mc_j(x) = z(j,x) \cdot F_{cM}(j,x) + (F_{cm}(j,x) \cdot k_{mx}(j,x)) \quad (8)$$

where:

Fig. 3. Simplification by symmetry of the problem: (a) Even number n_0 of transverse reinforcements, (b) Odd number n_0 of transverse reinforcements.

$F_{cM}(j,x)$: the equivalent discrete force caused by the distributed force due to the concrete cover in segment j, between position $z = z(j,x)$ and $z = L/2$.

$$F_{cMx}(j,x) = \alpha_c \int_{z(j,x)}^{L/2} g(z) \cdot dz \qquad (9)$$

$F_{cm}(j,x)$: the equivalent discrete force caused by the distributed force due to the concrete cover in segment j, between position $z = 0$ and $z = z(j,x)$.

$$F_{cmx}(j,x) = \alpha_c \int_0^{z(j,x)} g(z) \cdot dz \qquad (10)$$

$k_{mx}(j,x)$: the centre of gravity of equivalent discrete force $F_{cm}(j,x)$ compared to position $z = 0$.

$$k_{mx}(j,x) = \frac{\int_0^{z(j,x)} z \cdot g(z) \cdot dz}{\int_0^{z(j,x)} g(z) \cdot dz} \qquad (11)$$

By applying the hypothesis that $g(z)$ can approach a third-degree polynomial, it entails the direct solution of the differential equations system, and it is possible to approach $Mc_j(x)$ with sufficient accuracy. If greater accuracy is required, a solution must be considered by successive iterations and by updating displacement $g(z)$ from the displacements $y_j(x)$ obtained from the previous iteration. The solution of differential Eq. (1) for each segment j is:

$$y_j(x) = A_j \sin\left(\beta\frac{x}{s}\right) + B_j \cos\left(\beta\frac{x}{s}\right) + \frac{M_0 + M_{sj}(x) + M_{cj}(x)}{P} \qquad (12)$$

where:

A_j, B_j: the constants for each segment j.
β: $\beta = s\sqrt{\frac{P}{E_r I}}$

The values of constants A_j and B_j are obtained from the compatibility equations (13), if n_0 is even and (14) if n_0 is odd, among the displacements $y_j(x)$ in each segment j.

$$
\begin{array}{ll}
y_0(x=0) = 0 & y_0'(x=0) = 0 \\
y_0(x=s) = y_1(x=0) & y_0'(x=s) = y_1'(x=0) \\
\dots & \dots \\
y_i(x=s) = y_{i+1}(x=0) & y_i'(x=s) = y_{i+1}'(x=0) \\
\dots & \dots \\
y_{n-1}(x=s) = y_n(x=0) & y_{n-1}'(x=s) = y_n'(x=0)
\end{array}
\qquad (13)
$$

$$
\begin{array}{ll}
y_0(x=0) = 0 & y_0'(x=0) = 0 \\
y_0(x=s) = y_1(x=0) & y_0'(x=s) = y_1'(x=0) \\
\dots & \dots \\
y_i(x=s) = y_{i+1}(x=0) & y_i'(x=s) = y_{i+1}'(x=0) \\
\dots & \dots \\
y_{n-2}(x=s) = y_{n-1}(x=0) & y_{n-2}'(x=s) = y_{n-1}'(x=0)
\end{array}
\qquad (14)
$$

After determining constants A_j and B_j for each segment j, it is known that displacement $y_j(x)$, expressed in relation to the n unknown reactions F_j and to unknown bending moment M_0 acts at the built-in end. To obtain forces F_j and moment M_0, for each intermediate support j of the model (Fig. 3), condition (15) is applied for all the elastic supports (from $j = 1$ to n), and the symmetry condition is also applied (16).

$$y_j(x=0) = F_j/\alpha_s \quad \forall j = 1 \; to \; n \qquad (15)$$

$$
\left.
\begin{array}{ll}
\text{For } n_0 = 0 & y_0'\left(x = \frac{L}{2}\right) = 0; \\
\text{For } n_0 > 0 & \text{if } n_0 \text{ is even}: y_n'\left(x = \frac{s}{2}\right) = 0 \\
& \text{if } n_0 \text{ is odd}: y_{n-1}'(x = s) = 0
\end{array}
\right\}
\qquad (16)
$$

The $n + 1$ conditions ((15) and (16)) can be expressed according to transverse reinforcement separations s, and parameters β (17), γ (18) and k_{cs} (19). These $n + 1$ conditions make up a homogeneous system (20).

$$\beta = s\sqrt{\frac{P}{E_r I}} \qquad (17)$$

$$\gamma = \alpha_s s^3 / E_r I \qquad (18)$$

$$k_{cs} = \frac{\alpha_c}{\alpha_s} s \qquad (19)$$

$$c_c = \frac{\beta 2}{\pi^2} = \frac{P_c}{\pi^2 E_r I / s^2} = \frac{P_c}{P_0} \qquad (22)$$

$$M \cdot F$$

$$= \begin{pmatrix}
m_{11} & m_{12} & \cdots & m_{1i} & \cdots & m_{1n} & m_{1n+1} \\
m_{21} & m_{22} & \cdots & m_{2i} & \cdots & m_{2n} & m_{2n+1} \\
\cdots & \cdots & \cdots & \cdots & \cdots & \cdots & \cdots \\
m_{i1} & m_{i2} & \cdots & m_{ii} & \cdots & m_{in} & m_{in+1} \\
\cdots & \cdots & \cdots & \cdots & \cdots & \cdots & \cdots \\
m_{n1} & m_{n2} & \cdots & m_{ni} & \cdots & m_{nn} & m_{nn+1} \\
m_{n+11} & m_{n+12} & \cdots & m_{n+1i} & \cdots & m_{n+1n} & m_{n+1n+1}
\end{pmatrix}
\begin{pmatrix}
F_1 \\ F_2 \\ \cdots \\ F_i \\ \cdots \\ F_n \\ M_0
\end{pmatrix}$$

$$= \begin{pmatrix}
0 \\ 0 \\ \cdots \\ 0 \\ \cdots \\ 0 \\ 0
\end{pmatrix}$$

where:

P_0: critical load of the bar hinged between two consecutive supports
P_c: critical load on the bar

Fig. 4 shows the scheme of the followed procedure to obtain the limit values of γ and β when relation η and parameter k_{cs} are known. Relation η is linked to length L and transverse reinforcement separation s ($L = \eta \cdot s$). Fig. 5 shows abaci that provide adimensional critical load c_c according to parameters γ (18) and k_{cs} (19). The range of η in abaci is: $\eta = 0.3$ to $\eta = 5$. When η?1, the longitudinal reinforcement buckles between the transverse reinforcement and is considered a single segment ($j = 0$). In the opposite case ($\eta > 1$), some transverse reinforcement is involved in instability zone L.

With the results obtained after applying the procedure illustrated in Fig. 4, a least-squares fit is done which allows Eqs. ((23)–(25)) to be proposed to calculate adimensional critical load c_c. The k_{cs} values employed for this purpose fell between 0 and 30.

3.3. Solving the problem

According to the followed method to solve the differential equations system (20) proposed by Papia et al. [8] to analyse the instability of compressed bars on RC columns, reactions F_j and bending moment M_0 are calculated. Eq. (20) makes up a homogeneous equations system. To find a different solution to the trivial one, the determinant of matrix M ($D = \det(M)$) must be null.

As Papia et al. indicated [8], presence of a concrete core renders taking into consideration only the deflection shape of a symmetric type necessary. Consequently:

$$y_j(x) \geqslant 0 \quad \forall x, j \qquad (21)$$

Values β, γ and k_{cs} must fulfil condition (21). Once β and k_{cs} are known ($k_{cs} = 0$ from the case indicated in Papia et al. [8]), the maximum γ value is obtained for the limit condition of inverting the sign of the curvature at the built-in end. For this particular situation, the value of unknown quantity M_0 is null. This condition ($M_0 = 0$) is fulfilled by eliminating the row and column n + 1 from the equations system (20). The resulting equations system has unknown D quantities F_j and is homogeneous. Once again, in order to find a different solution to the trivial one, minor D_1 of order n of matrix M has to be null.

Consequently, knowing the length L where the instability of longitudinal bars takes place and parameter k_{cs}, which related cover stiffness α_c and transverse reinforcement stiffness α_s, the limit values of γ and β are obtained by imposing the condition of both determinant $D = 0$ and minor $D_1 = 0$. In both determinants (and D_1), separation s is the common factor. Consequently, they depend exclusively on β, γ and k_{cs}. Finally, a change in the variable regarding parameter β is made to obtain the adimensional critical load.
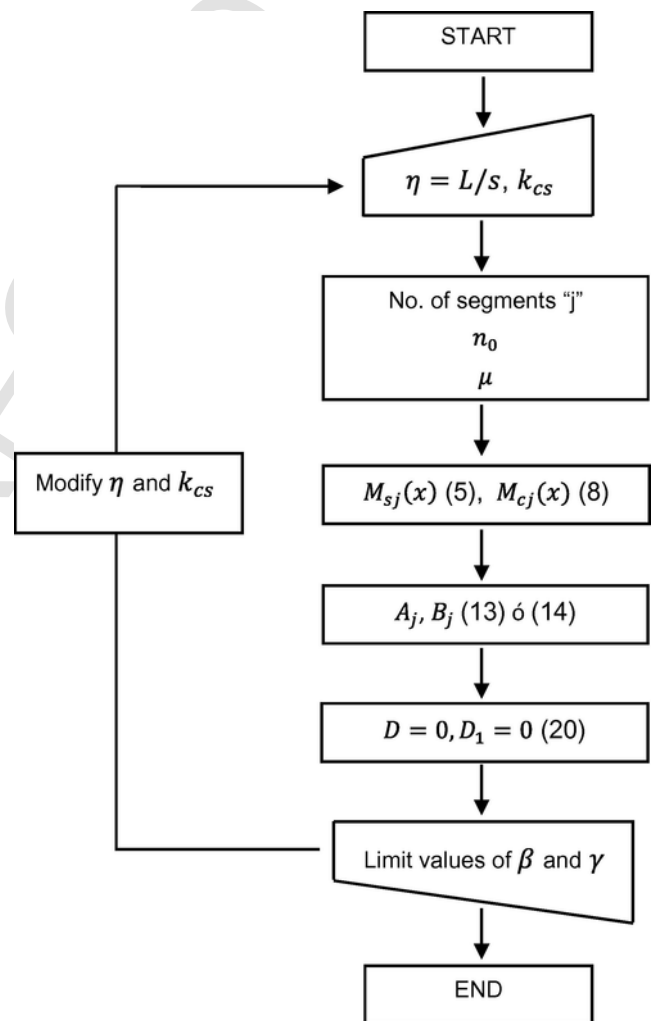
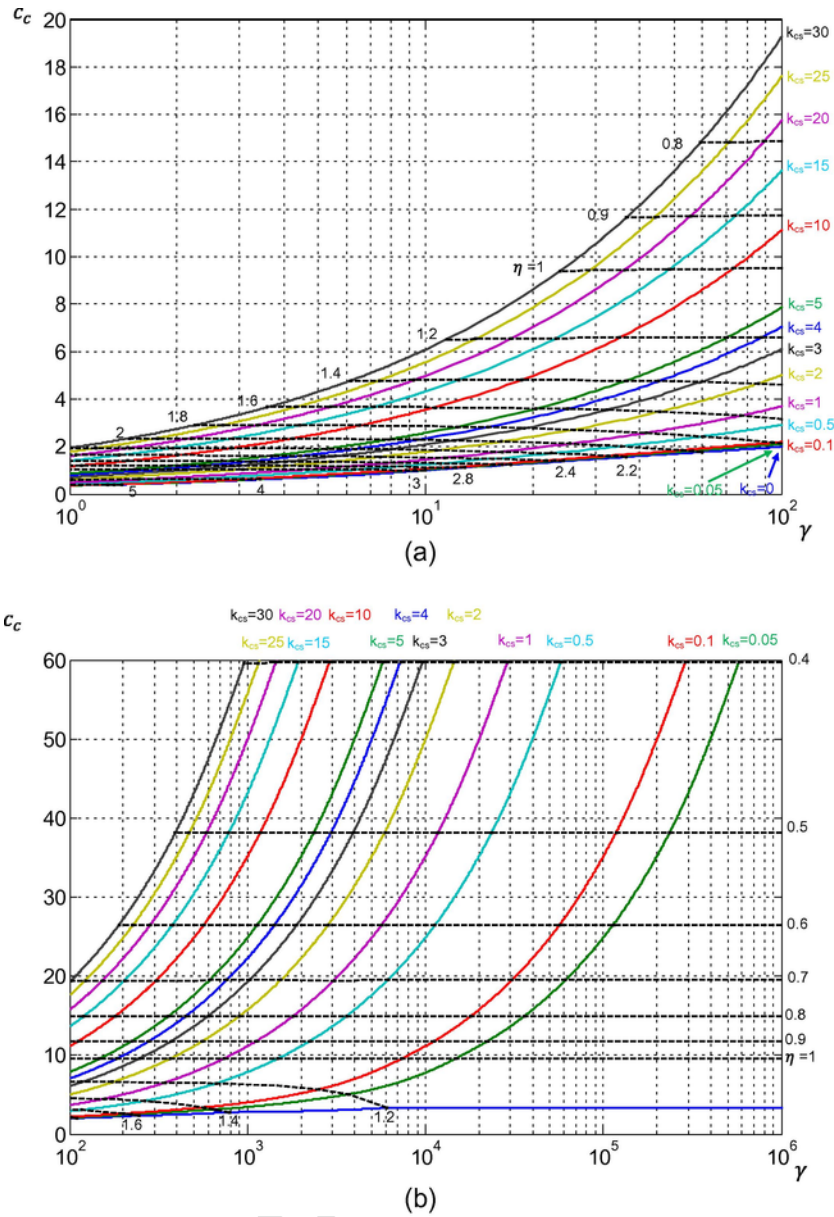Fig. 4. Flow chart to solve the differential equations systems at the deflected shape.

Fig. 5. Abaci to determine the adimensional critical load: (a) γ?100; (b) γ?100.

In the usual case of not contemplating the concrete cover ($k_{cs} = 0$), Eq. (23) is considered with determination coefficient $R'2 = 0.99$. For $0 < k_{cs} < 30$, two equations are proposed to improve accuracy: one for the curves below the line of $\eta = 1.4$ and another for those positioned above the line. The equation of this line is: $c_{c_{\eta=1.4}}(\gamma) = -0.00124(\log_{10}\gamma)^7 + 4.8$. The average of the co-efficient R^2 values, for each curve where k_{cs} is constant, is 0.99. For any k_{cs} values over 30, it is possible to rule out the influence of transverse reinforcements. In this case, a method is followed based on min-imising energy to calculate the critical load (Talaat and Mosalam [21], Campione [11]). The adimensional critical load obtained from this method is offered in Eq. (26).

$$k_{cs} = 0 \quad c_c = 4 \cdot \left(1 - \frac{1}{1 + 0.09\gamma^{0.58}}\right) \tag{23}$$

$$0 < k_{cs} \leqslant 30 \quad c_c = a_1 * e^{b_1 \cdot \log_{10}\gamma} + c_1 \quad if\, c_c \geqslant c_{c_{\eta=1.4}}(\gamma) \tag{24}$$

where:

$$a_1 = 0.35k_{cs}^{0.5} - 0.0066$$

$$b_1 = \frac{1.15k_{cs} + 0.035}{k_{cs} + 0.029}$$

$$c_1 = \frac{-0.0116k_{cs} + 0.062}{k_{cs} + 0.036}$$

$$c_c = a_2 * e^{b_2 \cdot \log_{10}\gamma} + c_2 \quad if\ c_c < c_{c_{\eta=1.4}}(\gamma) \tag{25}$$

where:

$$a_2 = \frac{5.5k_{cs}^3 + 99.3k_{cs}^2 + 189k_{cs} + 91.2}{k_{cs}^3 + 93k_{cs}^2 + 417k_{cs} + 25.4}$$

$$b_2 = \frac{1.14k_{cs}^2 + 1.26k_{cs} + 0.08}{k_{cs}^2 + 1.535k_{cs} + 0.404}$$

$$c_2 = \frac{-0.02k_{cs}^2 - 0.375k_{cs} - 1.07}{k_{cs}^2 + 5k_{cs} + 0.325}$$

$$k_{cs} > 30 \quad c_c = \left(\frac{s}{\pi}\right)^2 \sqrt{\frac{12\alpha_c}{E_r I}} \tag{26}$$

3.4. Transverse reinforcement stiffness

To calculate adimensional critical axial load c_c, it is necessary to know transverse reinforcement stiffness α_s and concrete cover stiffness α_c. Concrete cover stiffness α_c depends on the concrete type. This stiffness must be calibrated using experimental data.

According to Papia et al. [8], transverse reinforcement stiffness α_s is calculated by the following equation:

$$\alpha_s = \frac{E_{sw} \cdot A_{sw}}{L_{ef}} \tag{27}$$

where:

E_{sw}: the tangent elasticity module of the transverse reinforcement
A_{sw}: the transverse reinforcement area
L_{ef}: the effective transverse reinforcement length, a function of the reinforced configuration and load type (concentric or eccentric)

Elasticity module E_{sw}, which is considered in the stiffness α_s calculation, depends on whether the transverse reinforcement is yielded or not. So, it is necessary to know the transverse reinforcement strain that occurs as a result of the transverse concrete expansion. This strain is related with the longitudinal strain through the dilatancy parameter (Khajeh and Attard [22], Lokuge et al. [23], Montoya et al. [24], Osorio et al. [25]).

Parameter L_{ef} of Eq. (27) varies according to the arrangement of transverse reinforcements and the type loading (concentric or eccentric). Fig. 6 shows various transverse reinforcement configurations and the equation L_{ef}, where transverse reinforcement bending stiffness is ruled out.

4. Comparing the proposed model with other models

This section compares the results obtained by applying the model proposed herein with the results of applying the analytical models, both discrete and continuous, proposed by Papia et al. [8], Talaat and Mosalam [21] and Campione [11].

Fig. 7(a) represents an example of critical buckling stress of compressed passive reinforcements according to separation s among the transverse reinforcements for a 20×20 cm cross section with four 12 mm-diameter longitudinal reinforcements and 6 mm-diameter
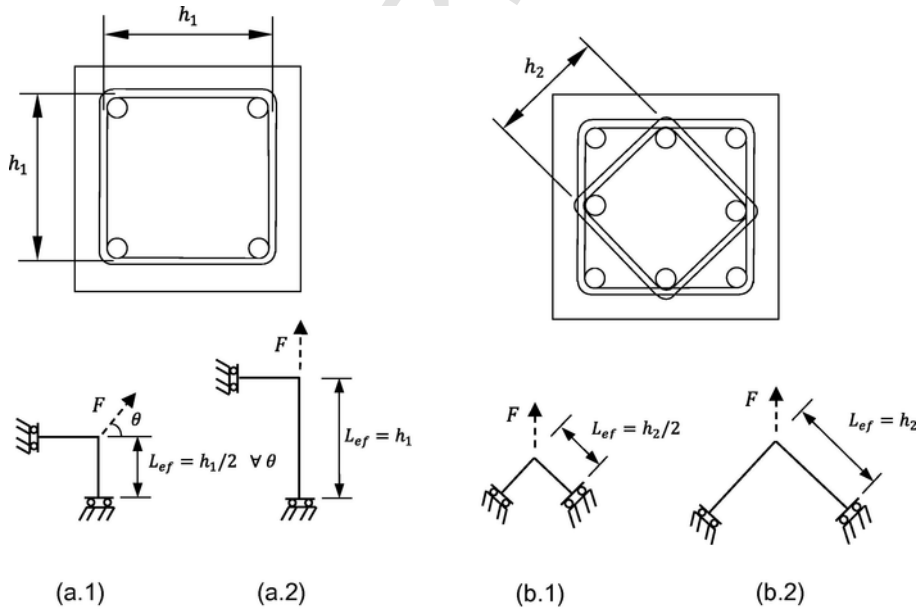

Fig. 6. Effective lengths of stirrups with the usual configurations: (a.1) Corner bars for concentric loading (Papia et al. [8]), (a.2) Corner bars for eccentric loading (b.1) Middle bars for concentric loading (Papia et al. [8]), (b.2) Middle bars for eccentric loading.
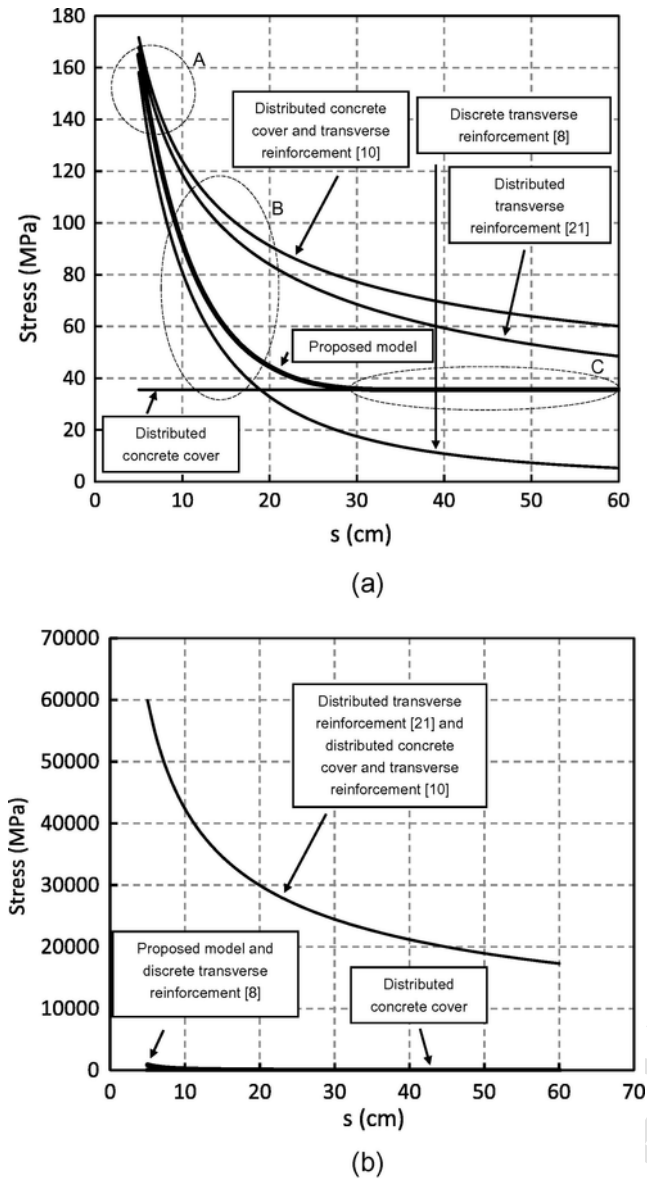
Fig. 7. Critical stress–transverse reinforcements separation according to several methods: (a) Stirrups in post-yield branch, (b) Stirrups in elastic branch.

transverse reinforcements. The employed mechanical parameters are: α_s = 0.236 N/mm, α_c = 0.211 MPa, E_r = 6263.9 MPa.

For separations of more than 30 cm, the proposed model coincides with the distributed model when only concrete cover stiffness is considered (zone C in Fig. 7(a)). This is because the longitudinal reinforcement buckles between transverse reinforcements and the transverse reinforcement has no effect. Conversely, when the separation among transverse reinforcements comes close to zero, the proposed model coincides with those that consider the transverse reinforcement as both discrete and distributed forms (zone A in Fig. 7(a)). There are two reasons for this: the cover no longer had a main effect and the small transverse reinforcement separation (s ≈ 5 cm) allows the distributed transverse reinforcements hypothesis to be considered. However, when the separations among transverse reinforcements do not coincide with former cases, the models that consider distributed transverse reinforcements overestimate the critical buckling stress, while those that contemplate only the concrete cover underestimate

this (zone B in Fig. 7(a)). The model of Papia et al. [8] offers a lower critical stress rate by assuming that k_{cs} = 0.

The employed value of α_s supposes that the stirrups are yielded. In the case that the stirrups are not yielded (α_s = 30,000 MPa) Fig. 7(b) is obtained. In this figure the same methods used in the Fig. 7(a) are represented. On the one hand, the energetic approaches (Talaat and Mosalam [21] and Campione [11]), which consider the stirrups distributedly along the buckling length, proportionate very high values of buckling stress. This is due to the fact that the elastic stiffness α_s is very high. On the contrary, the buckling stress with the Papia and the proposed method (both of them coincide because of k_{cs}≈0 if concrete cover is degraded and stirrups are in elastic range) is quite lower than in the previous cases. This is why stirrups are considered discretely in these models and, consequently, the reinforcement can buckle between the stirrups or barely deforming them if buckling length is little higher than stirrups separation.

5. Comparing the proposed model with the experimental results

An experimental programme was run to study the local instability of the compressed bars in the RC columns under eccentric loading, manufactured in conventional concrete (with and without fibres) and to calibrate the proposed analytical model, specifically for cover stiffness α_c.

5.1. Specimens

Nine eccentrically loaded RC columns (known as dog-bone-shaped) are tested under eccentric loading. The geometry and details of the reinforcement arrangement are provided in Fig. 8. Two plaques are screwed into the ends of the column. Each plaque has a groove. The load is applied through the knife edges seated in these grooves. The boundary conditions at the ends are both hinges and the eccentricity of 0.10 m are equal and of the same sign. The free length among hinges is 1.39 m. The test is designed so that the column achieves failure by the concrete with no high plastic strain developing in the tensioned reinforcement. This is why the longitudinal reinforcement is not symmetrical to the bending axis. The longitudinal reinforcements are 12 mm and 16 mm in diameter on the compressed and the tensioned face, respectively. With this asymmetrical longitudinal reinforcement configuration, the compressed longitudinal reinforcement is able to reach high compression strains without the tensioned reinforcement undergoes remarkable plastic deformations. In this way, it is assured that the buckling is produced. The cross section is square (0.20 × 0.20 m) at the centre of the column.

The main purpose of these tests is to investigate the effects of the transverse reinforcement separation (0.05, 0.10, 0.30 m) and the steel fibre content in the concrete mass (0, 40 and 80 kg/m³) on the NSC column, whose average strength is 25 MPa.

Therefore, the following three s/d_b ratios were considered: 4.16, 8.33 and 25, where d_b is the diameter of compressed longitudinal reinforcement (12 mm) and s is the transverse reinforcement separation (0.05, 0.10, 0.30 m). The ratio s/d_b = 4.16 is lower than the maximum ratio given by EN 1998-1:2004 [2] for high ductility columns (DCH) or by ACI 318R-14 [4] for special frames, which is in both codes s/d_b = 6. The ratio s/d_b = 8.33 is approximately equal to the ratio proposed by EN 1998-1:2004 [2] for medium ductility columns or by ACI 318R-14 [4] for columns of ordinary frames, which is in both codes s/d_b = 8. Finally, the ratio s/d_b = 25 is higher than the ratio of EN 1992-1:2004 [26], EN 1998-1:2004 [2] and ACI-318 [4] codes, whose maximum value is s/d_b = 20. The objective of this last case is
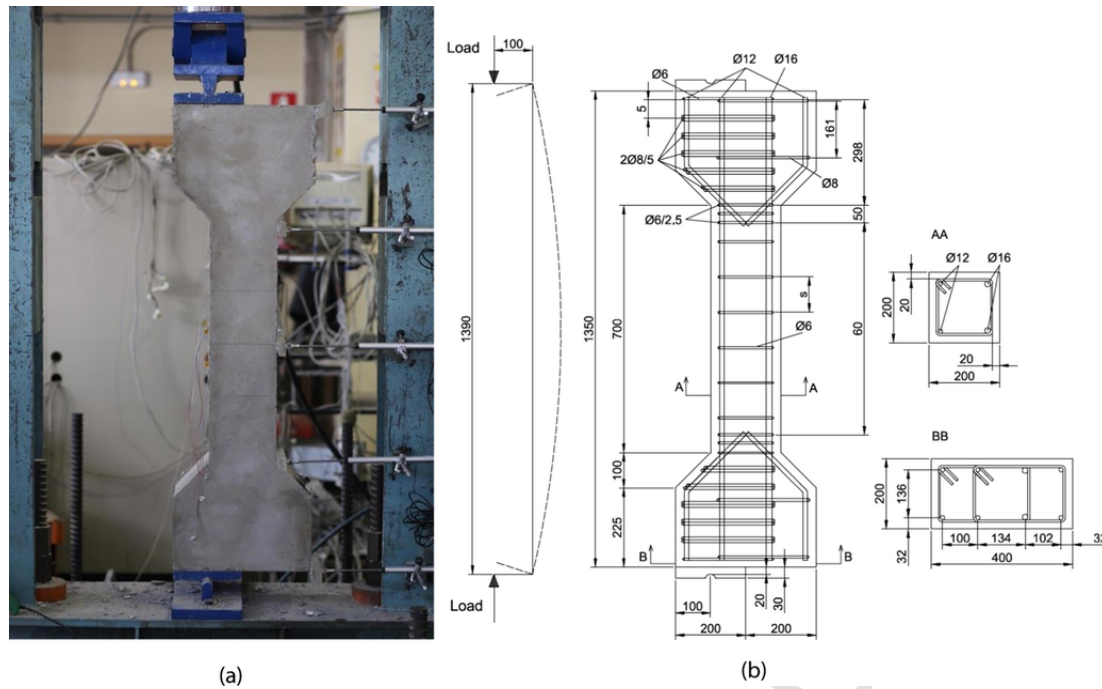
Fig. 8. Details and arrangement of specimens: (a) The outer configuration in tests, (b) Scheme of the reinforcement arrangement (rates in mm).

to analyze how fibre reinforced concrete is able to delay the compressed reinforcement buckling when buckling happens between two stirrups, with a high transverse reinforcement separation.

Table 3 offers details of the nine columns included in the experimental programme. Specimens are denoted as: C25FxSy, where "x" indicates fibre content (0, 40 and 80 kg/m^3) and "y" denotes transverse reinforcement separation (5, 10 and 30 cm).

Specimens are made horizontally on a vibrator table, are unmoulded 24 h after concreting, are placed in a humid atmosphere to minimise retraction effects, and are placed horizontally. All the specimens are tested 28 days after being produced. Strength to the concrete compression of each column is obtained as the average of three cylindrical control specimens that measure 150 × 300 mm (UNE-EN 12390-3 [27]).

5.2. Material characterisation

To manufacture concrete, a commercial product is used: Sikacrete®-08 SCC. This material is a self-compacting concrete whose measured strength is 25 MPa and its slump flow is 670 mm. The steel fibres used are DRAMIX 80/30 BP, 30 mm long with a slenderness of 80, a tensile strength of 3070 MPa and an elasticity module of 200 GPa.

A prismatic control specimen is manufactured for each element, which measure 550 × 150 × 500 mm, to determine the residual flexural tensile strength according to standard UNE EN 14651:2007 [28]. Table 2 presents the results obtained with the control standard of the materials, where f_{cm} is the average compressive strength of concrete (UNE-EN 12390-3 [27]), E_c is the elasticity module of concrete, ε_{c85} is the strain that corresponds to a stress of 0.85 f_{cm} denoted after a peak load (measured on the softening branch), f_{LOP} is the proportionality limit, $f_{R,1}, f_{R,2}, f_{R,3}$ and $f_{R,4}$ are the residual tensile strengths corresponding to Crack Mouth Opening Displacement (CMOD) of 0.5, 1.5, 2.5 and 3.5 mm, respectively, in the flexural tensile strength test (UNE EN 14651:2007 [28]).
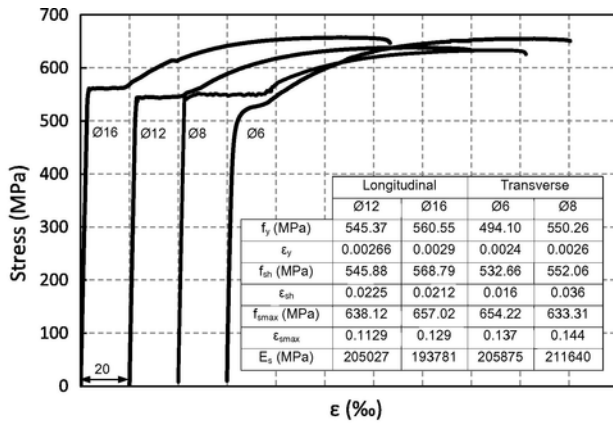
Table 2
Mechanical characteristics of concrete.

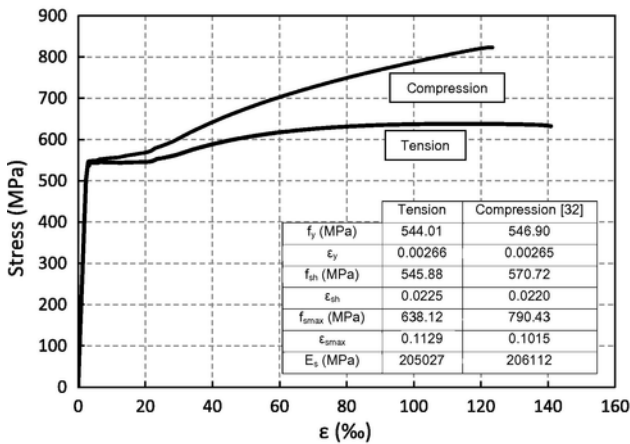| Specimen	f_{cm} (MPa)	E_c (MPa)	ε_{c85} (‰)	f_{LOP} (MPa)	$f_{R,1}$ (MPa)	$f_{R,2}$ (MPa)	$f_{R,3}$ (MPa)	$f_{R,4}$ (MPa)
C25F00S30	28.25	26,584	4.4	–	–	–	–	–
C25F00S10	24.17	25,200	4.8	–	–	–	–	–
C25F00S05	23.16	25,131	3.8	–	–	–	–	–
C25F40S30	21.56	23,435	–	1.78	2.1	2.18	1.87	1.43
C25F40S10	24.56	23,897	–	1.87	2.19	2.08	1.77	1.43
C25F40S05	25.25	24,249	–	1.91	2.39	1.97	1.66	1.54
C25F80S30	25.52	24,225	–	3.60	4.91	5.45	5.17	3.57
C25F80S10	29.16	26,300	–	3.72	4.95	5.6	5.21	3.66
C25F80S05	20.89	22,690	–	3.47	4.71	5.7	5.29	3.43

Steel of quality B500SD (EHE-08 (2008)) and class C (EN1992-1-1:2004 is employed [26]). The characterisation test results in the longitudinal and transverse reinforcement tensile tests (UNE EN-10002-1 [29]) are shown in Fig. 9(a), where f_y, ε_y, f_{sh}, ε_{sh}, f_{smax}, ε_{smax}, E_s, are the yield stress, the strain that corresponds to the yield stress, the stress at which the hardening branch begins, the stress associated with ε_{sh}, the maximum stress, the strain associated with the maximum stress and the elasticity modulus, respectively. In the 12-mm reinforcements, the compression characteristics are obtained by following the procedure used by Dodd and Restrepo-Posada [30] (Fig. 9(b)).

5.3. Instrumentation

On each column, strain gauges are arranged on both the longitudinal and transverse reinforcements, and on the compressed face of the concrete (Fig. 10). The gauges placed on compressed and tensioned reinforcements are arranged equidistantly among stirrups in three sections (the central ones). The gauges of the concrete compressed area are arranged only in the midspan section. To avoid the local effect of bar curvature, gauges have to be arranged perpendicularly to the bending axis (on the lateral bar faces). Nonetheless,

	Longitudinal		Transverse	
	Ø12	Ø16	Ø6	Ø8
f_y (MPa)	545.37	560.55	494.10	550.26
ε_y	0.00266	0.0029	0.0024	0.0026
f_{sh} (MPa)	545.88	568.79	532.66	552.06
ε_{sh}	0.0225	0.0212	0.016	0.036
f_{smax} (MPa)	638.12	657.02	654.22	633.31
ε_{smax}	0.1129	0.129	0.137	0.144
E_s (MPa)	205027	193781	205875	211640

(a)

	Tension	Compression [32]
f_y (MPa)	544.01	546.90
ε_y	0.00266	0.00265
f_{sh} (MPa)	545.88	570.72
ε_{sh}	0.0225	0.0220
f_{smax} (MPa)	638.12	790.43
ε_{smax}	0.1129	0.1015
E_s (MPa)	205027	206112

(b)

Fig. 9. Mechanical properties of reinforcements: (a) Stress-strain behaviour of steel reinforcements, (b) Tensioned and compressed constitutive curve of the 12 mm diameter longitudinal reinforcements.
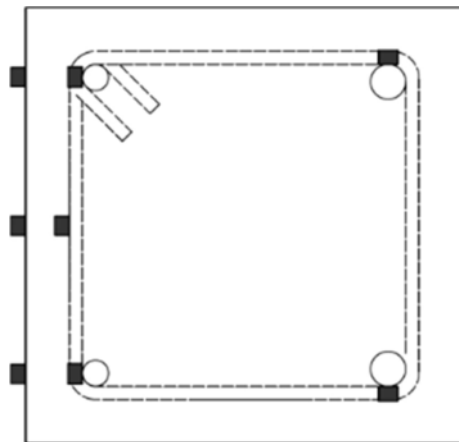

Fig. 10. Strain gauge layout.

to be able to detect the change in the compressed bar curvature under local buckling, the gauge is placed in parallel to the bending axis and on the side of the cover. As it is well-known, strains grow with the applied load in an eccentric load test through growing displacements (Fig. 11, point a). When the peak load is reached, a plastic hinge

forms. On the softening branch in the load-strain diagram, despite the load diminishing, the strains in the critical section keep increasing because displacement grows. As a result, the strain of the compressed reinforcement located in the yielding zone increases throughout the test (Fig. 11, point b), provided that the neutral fibre of the section is below it. If the compressed reinforcement undergoes local buckling, the compression gauge detects any increased tensile strain (Fig. 11, point c), and can lead to tensile strain due to an excess change in the curvature, although the reinforcement is placed in the compression area of the section (Fig. 11, point d).

Five linear voltage displacement transducers (LVDTs) are placed at 0, 325, 675, 1025 and 1350 mm from the lower specimen end. A synchronised recording system is used to assign the corresponding applied load to each photogram. As strain gauges are arranged on the compressed bars, in order to capture buckling and not the average strain, the bar strain in the buckling area is obtained from both the tensioned bar and the position of the neutral fibre obtained by analysing photographs.

5.4. Test set up

A 2500 kN hydraulic actuator is employed. A test is performed with displacement control in the midspan section at a speed of 0.2 ± 0.05 mm/min.

6. Results and discussion

Fig. 12 shows the diagram that relates the normalised vertical load ($v = N/(A_c f_c)$, where N is the load applied by the hydraulic actuator, A_c is the gross area of section and f_{cm} is the average strength to compression) with longitudinal reinforcement strain (ε_l) in the zone where instability of compressed bars occurred. Fig. 13 shows the normalised vertical load (v) – normalised displacement diagrams (Δ/L_{tot}, where Δ is the displacement in the midspan and L_{tot} is the distance among the hinges of the load). The point where compressed reinforcement buckled is marked in Fig. 13. The results are grouped according to the fibre content in the concrete mass. Table 3 provides the experimental results of the peak load and of the instability situation of compressed bars.

As expected, the peak load capacity of the columns increased slightly when fibre content increased and when the stirrups separation reduced due to increased confinement. Regarding the post-peak branch slope, the smaller the separation among stirrups, the lower the absolute value of this slope became. The absolute value of the softening branch slope also lowered with fibre content.

Fig. 14 depicts the cracking patterns of the specimens. In all cases, the cracking on the visible tension area began to take place at the stirrups level. With the plain concrete, two large cracks formed in the tension area when the compression zone was damaged and a plastic hinge formed. For concretes with fibres, the crack width was smaller with fibre content and the number of cracks increased, which formed more distributed cracking. The cracking in the compressed zone was longitudinal and more distributed when fibre content increased. When these cracks were noticeable, the plastic hinge began to form and cracks opened more widely as rotation increased.

From the strain (ε_{crit}) results and the critical buckling stress (σ_{crit}) results (Table 3), which stemmed from the stress-strain ratio under compression (Fig. 9(b)), differences in behaviour between the concretes with and without steel fibres were found. For the plain concrete, compressed reinforcement buckling took place after concrete cover spalling. This situation occurred approximately when the compressed reinforcement strain was ε_{c85} (the strain that corresponded to
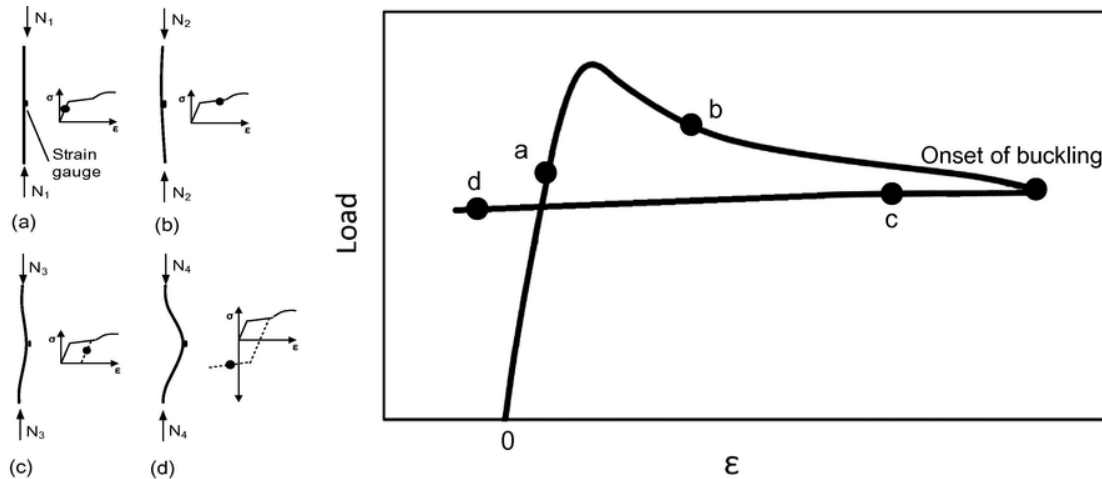
Fig. 11. Methodology proposed to detect buckling on the compressed bar.

a stress $0.85 \cdot f_c$ after the peak load) (Table 2). Campione also reached this conclusion [31]. Given this situation, the transverse reinforcement itself would be able to avoid the compressed reinforcement strain. If transverse reinforcement stiffness was insufficient, buckling would occur along with cover spalling (C25F00S30 and C25F00S10). If it was sufficient, however, reinforcement buckling would not occur simultaneously with cover spalling. Thus with specimen C25F00S05, whose stirrups separation was 5 cm, critical strain was much greater than ε_{c85} because the transverse reinforcement prevented buckling from happening simultaneously with cover spalling.

For the concrete with steel fibres, the fact that the concrete mass had fibres increased the strain at which the reinforcement buckled (Table 3). Similar behaviour occurred between the pairs of specimens whose transverse reinforcement separation was 10 cm and 30 cm (C25F40S10-C25F40S30 and C25F80S10-C25F80S30) because the reinforcement among stirrups buckled in both cases. The buckling strain increased between these pairs when the fibre content in concrete was higher. The specimens with a transverse reinforcement separation of 5 cm (C25F40S05-C25F80S05) underwent greater strains (ε_{crit}) than those with α_c separations of 10 cm and 30 cm because the stiffness of stirrups was greater.

All the specimens with transverse reinforcement separations of 5 cm underwent similar ε_{crit} strains, regardless of them having fibres or not. In such cases, this was justified by the transverse reinforcement being capable of restraining buckling, even when the concrete cover spalled (plain concrete) or proved ineffective for high degradation situations (concrete with fibres).

6.1. Concrete cover stiffness α_c calibration

According to the experimental results, with the plain concrete elements, stiffness of calibration was not necessary because compressed reinforcement buckling took place after concrete cover spalling had occurred. Consequently, $\alpha_c = 0$ ($k_{cs} = 0$) was used to assess critical buckling stress (23) in the plain concrete elements.

However, with the elements made in concrete with steel fibres, the stiffness of concrete cover α_c had to be considered. As the tests showed, stiffness α_c depended on the level of strain and, consequently, on the degradation of the cover. The α_c value was obtained from the results of both the experiments and the proposed analytical model ((24)–(26)). Fig. 15 illustrates the stiffness of cover α_c that corresponded to the instability of bars. A value of $\alpha_c = 70$ MPa was determined, irrespectively of $f_{R,1}$.

Fig. 15 also shows the relation between the compressed bar strain in the instability situation ($\varepsilon_{crit,\eta \leq 1}$) and strength $f_{R,1}$ for only the cases of 10 cm and 30 cm stirrups separations, where η?1 (the reinforcement bucked among stirrups). Therefore, $\varepsilon_{crit,\eta ?1}$ is the buckling strain of the compressed steel reinforcements that buckle between the stirrups. It is the strain of the longitudinal reinforcement buckling of the specimens where only the concrete cover stiffness α_c contains the buckling until it is finally produced due to the concrete cover degradation. The following Eq. (28) is proposed based on experimental results, where $\varepsilon_{crit,\eta \leq 1}$ is expressed as ‰ and $f_{R,1}$ in MPa.

$$\varepsilon_{crit,\eta \leqslant 1} = 0.66 \cdot f_{R,1} + 7.15 \tag{28}$$

Longitudinal reinforcement strain $\varepsilon_{crit,\eta \leqslant 1}$ was a limit strain for which the α_c value was known ($\alpha_c = 70$ MPa) since η?1 (only the cover contained buckling). Having exceeded strain $\varepsilon_{crit,\eta \leqslant 1}$, $\alpha_c < 70$ MPa was obtained because the cover presented greater degradation. So $\alpha_c = 0$ was taken for security reasons.

Finally, when stirrup separations were 5 cm, and where $\eta > 1$ (reinforcement buckling involved a longer length than the separation among stirrups), the critical strain that reached ε_{crit} did not only depend on concrete with a fibre content, but also on the stiffness of stirrups α_s. In these cases, the critical reinforcement strain was greater than in the cases with bigger separations ($\varepsilon_{crit} > \varepsilon_{crit,\eta \leqslant 1}$ (28)), provided α_s sufficed to delay the buckling of strains that exceeded $\varepsilon_{crit,\eta \leqslant 1}$. In these cases, once again a stiffness of $\alpha_c = 0$ was taken.

### 6.2. Verification of the model based on the experimental results

By applying the proposed analytical model ((23)–(26)), it was possible to obtain critical compressed bar stress σ_{crit}, where $\sigma_{crit} = c_c \cdot P_0 / A_s$ and where A_s was the area of this bar. As Talaat and Mosalam indicated [21], buckling onset ($\varepsilon_{crit,model}, \sigma_{crit,model}$) is determined when the critical stress–strain line intersect the stress–strain constitutive behaviour line. This critical line was generated by evaluating σ_{crit} at each axial strain increment (ε_l). According to the results in Tables 2 and 3, and also to proposed analytical model, a procedure was proposed to find both stress and strain on the longitudinal buckled bar based on successively increasing longitudinal bar strains (ε_l) until critical stress (σ_{crit}) equalled the current compressive stress (Fig. 9(b)). Two methodologies were proposed, one for concrete with fibres and another for plain concrete, as a result of the different behaviour
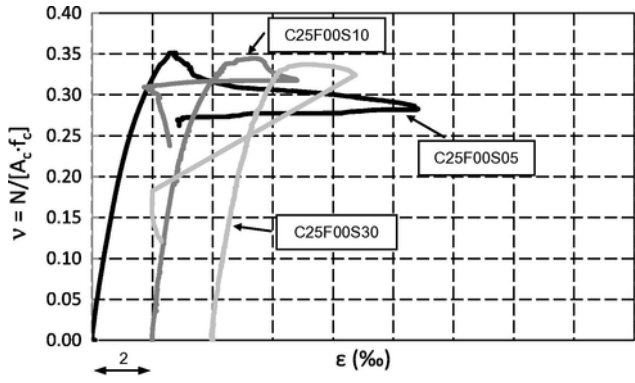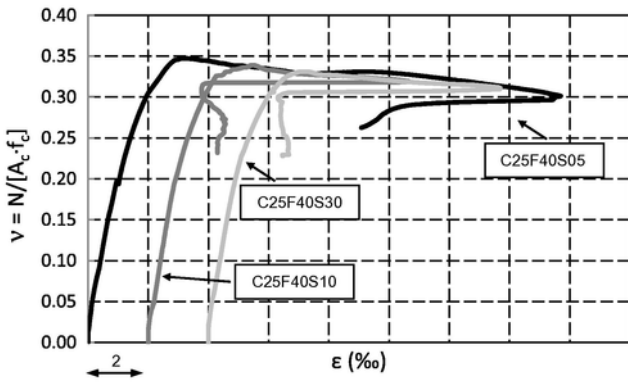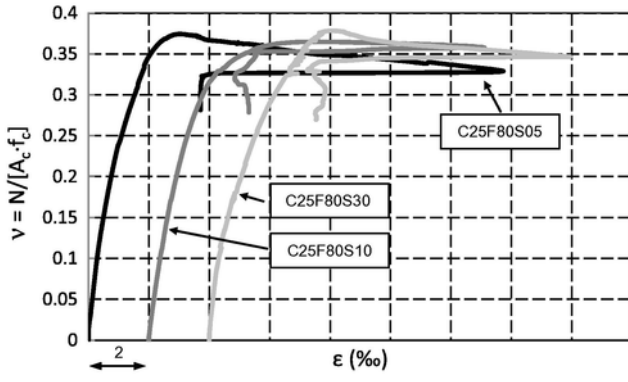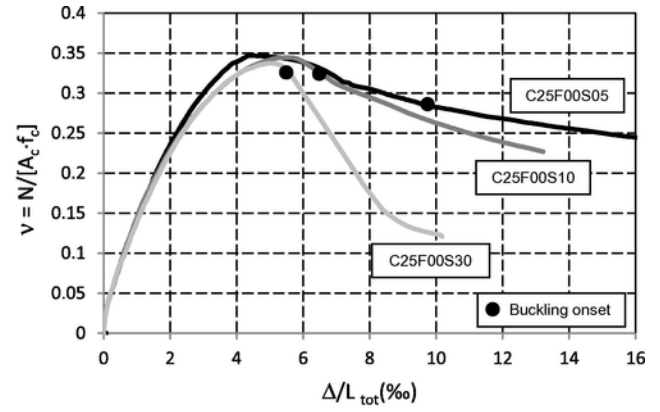
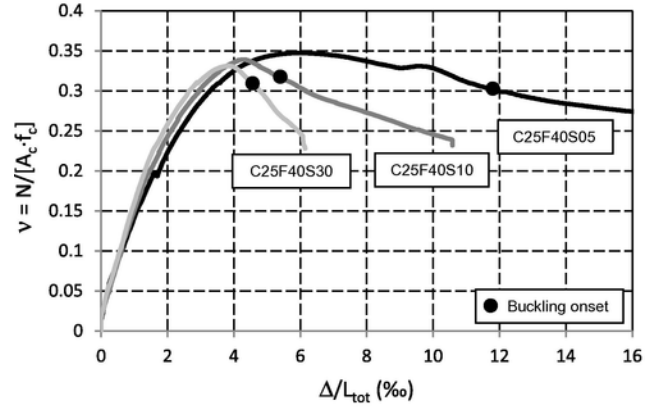**Fig. 12.** Normalised load–axial strain (v–ε) for columns under eccentric loads, (a) Plain concrete, (b) With 40 kg/m^3, (c) With 80 kg/m^3.

Fig. 13. Normalised load–normalised displacement (v–Δ/L) for columns under eccentric loads, (a) Plain concrete, (b) With 40 kg/m^3, (c) With 80 kg/m^3.

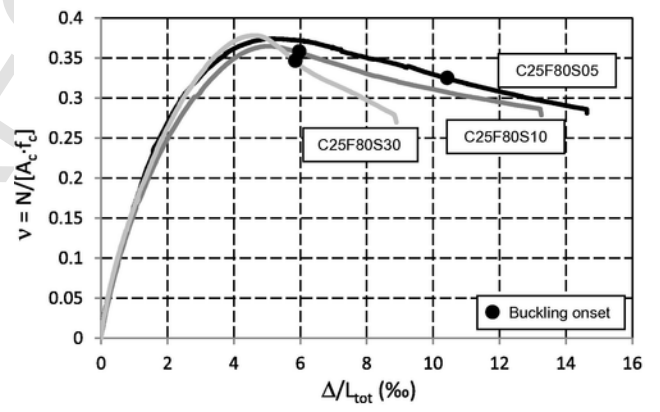observed in the experimental results (Tables 2 and 3).For the plain concrete, the procedure was as follows:

1. Assume longitudinal reinforcement strain (ε_l) equalled or was above ε_{c85}.
2. Calculate critical buckling stress (σ_{crit}) with the proposed analytical model, where $\alpha_c = 0$. As α_s depends on the tangent elasticity model of the transverse reinforcement, knowing whether the yielded state had been reached was necessary. To this end, adopting a dilatancy criterion was proposed (Khajeh and Attard [22], Lokuge et al. [23], Montoya et al. [24], Osorio et al. [25]) to know transverse reinforcement strain (ε_t) according to longitudinal strain (ε_l), and to compare it with the yield strain of trans-

verse reinforcement (ε_{ty}). Fig. 16(a) shows that α_s had to be used in each situation.

3a. If $\sigma_{crit} > \sigma_s(\varepsilon_l)$, where $\sigma_s(\varepsilon_l)$ was the reinforcement stress associated with strain ε_l, then the reinforcement did not buckle. In this case, the procedure had to be repeated by assuming a greater strain ε_l.

3b. When $\sigma_{crit} \leqslant \sigma_s(\varepsilon_l)$, then the reinforcement buckled. The buckling stress and strain were $\sigma_s(\varepsilon_l)$ and ε_l of the present iteration, respectively.

The procedure explained above was based on the compressed rein-

Table 3
Results of the experimental campaign and comparison with the proposed model.

	Experimental results						Proposed model results	
	Peak load		Instability situation of compressed bars				Instability situation of compressed bars	
Specimen	N_{max} (kN)	δ (mm)	N_c (kN)	δ (mm)	ε_{crit} (‰)	σ_{crit} (MPa)	$\varepsilon_{crit,model}$ (‰)	$\sigma_{crit,mo}$ (MPa)
C25F00S30	381.03	7.00	366.52	7.99	4.44	550.34	4.4	550.3(
C25F00S10	333.18	7.66	297.63	8.68	4.50	550.41	4.8	550.7(
C25F00S05	325.64	4.03	261.78	13.55	10.33	557.18	2.5	516.6'
C25F40S30	285.63	5.34	268.18	6.26	9.15	555.81	8.536	555.1(
C25F40S10	333.18	5.98	313.18	7.22	8.05	554.53	8.596	555.1'
C25F40S05	350.89	8.32	283.46	16.4	14.65	562.19	8.728	555.3:
C25F80S30	386.23	6.44	353.77	8.13	9.97	556.76	10.391	557.2:
C25F80S10	425.54	6.96	417.00	8.34	10.84	557.77	10.418	557.28
C25F80S05	312.78	7.16	308.01	14.73	12.83	560.08	10.259	557.1(

forcement strain and was, therefore, independent of the cover thickness. With the concrete with fibre content, the procedure was as follows:

1. Assume longitudinal reinforcement strain (ε_l).
2. Calculate critical buckling stress (σ_{crit}) with the proposed analytical model. For conventional concrete with steel fibres, the proposed stiffness of $\alpha_c = 70$ MPa was used if ε_l was below or equals critical strain $\varepsilon_{crit,\eta\leq l}$. If strain $?_l$ exceeded $\varepsilon_{crit,\eta\leq l}$, then $\alpha_c = 0$. Fig. 16(b) schematically shows values α_c and α_s that had to be used in each situation.
3a. If $\sigma_{crit} > \sigma_s(\varepsilon_l)$, then no reinforcement buckling took place. In this case, the methodology had to be repeated by assuming a greater strain ε_l.
3b. When $\sigma_{crit} \leq \sigma_s(\varepsilon_l)$, then reinforcement buckling took place. The buckling stress and strain were $\sigma_s(\varepsilon_l)$ and ε_l of the current iteration, respectively.

In order to consider the procedure with concretes with fibre content, the following requirements were: concrete cover thickness had to be sufficient so that fibres sewed the reinforcement to the concrete core; concrete residual tensile strengths $f_{R,1}$ and $f_{R,3}$ could not be below 40% and 20% of the proportionality limit (f_{LOP}), respectively, for fibres to have a structural function (EHE-08 [1]).

As with the procedure described for plain concrete, the criterion based on compressed reinforcement strains was also adopted for concretes with fibres. This procedure did not depend on section width because in the instability of bars situation, the concrete of the cover degraded and longitudinal cracking appeared on the compressed face

(Fig. 17). Table 3 compares the results obtained from the proposed procedure to the experimental results.

It was noteworthy that when both the above-described procedures were applied on concretes with and without fibres, high sensitivity of critical buckling stress was observed for minor variations in stirrup separations in the specimens that had 5 cm stirrup separations.

With all the tested specimens, the buckling strain was always below the strain where steel reached the hardening branch (ε_{sh}) (Table 3). Therefore to obtain the results shown in Table 3, reduced module E_r (2) was calculated by bearing in mind E_s and E_h, where E_s was the initial elasticity module and E_h was the elasticity module of the plastic branch prior to hardening (Fig. 9). The reduced elasticity module result was $E_r = 4793.5$ MPa. The adopted dilatancy criterion was that of Lokuge et al. [23].

7. Summary and conclusions

This work proposes a mixed analytical model to determine critical buckling loads in compressed reinforcements in concrete elements. This model is valid for monotonic loading, any transverse reinforcement distribution and separation, and for elements manufactured in concrete with or without fibres. Simplified equations are proposed to determine critical buckling load and the results are provided as abaci.

– The proposed model was calibrated to be applied to NSC columns with and without fibres under eccentric loading according to the experimental test results.
– The following conclusions were drawn from the obtained experimental results:
– For columns manufactured without steel fibres, if the reinforcement strain did not exceed ε_{c085}, the reinforcement did not buckle. If it exceeded $?_{c085}$, the concrete cover spalled ($\alpha_c = 0$) and critical buckling stress depended on transverse reinforcement stiffness.

For concretes with fibre content, if the compressed reinforcement strain was below a limit value ($\varepsilon_{crit,\eta\leq l}$), both concrete cover stiffness and transverse reinforcement stiffness were taken into account. Otherwise, only transverse reinforcement stiffness was considered ($\alpha_c = 0$). In all cases, the transverse reinforcement stiffness (α_s) varied according to whether it was yielded or not. An experimental methodology is proposed to determine the longitudinal reinforcement buckling stress and buckling strain.

Finally, a procedure to apply the mixed analytical model is proposed to determine the critical buckling load of conventional concrete (with or without fibres) columns under monotonic loading which considers any possible contribution of the concrete cover. This pro-
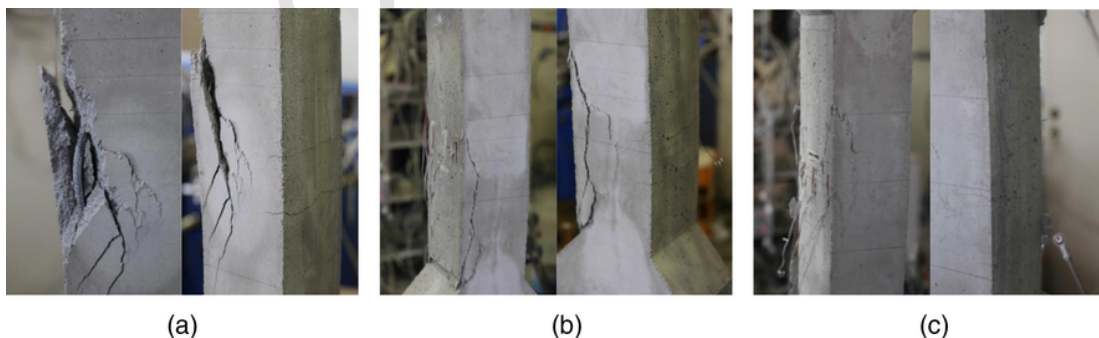

(a)   (b)   (c)

Fig. 14. Examples of specimen states after the test (a) Plain concrete, (b) With 40 kg/m³, (c) With 80 kg/m³.
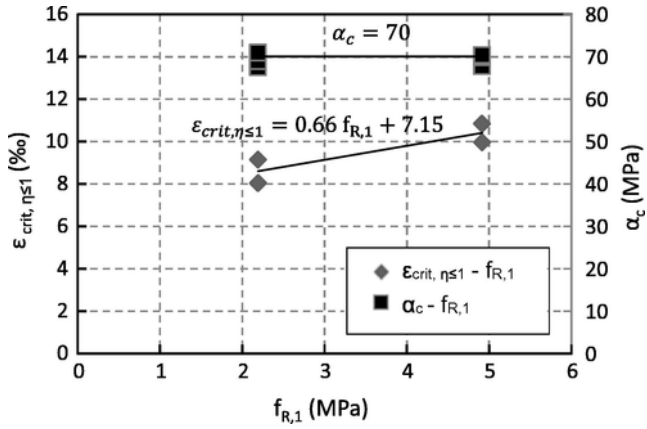
Fig. 15. Compressed bar strain in the instability situation ($\varepsilon_{crit,\eta\leq1}$) − residual tensile strength $f_{R,1}$ (left); concrete cover stiffness α_c − residual tensile strength $f_{R,1}$ (right).

cedure was used to verify the proposed model based on the experimental results.

8. Uncited references
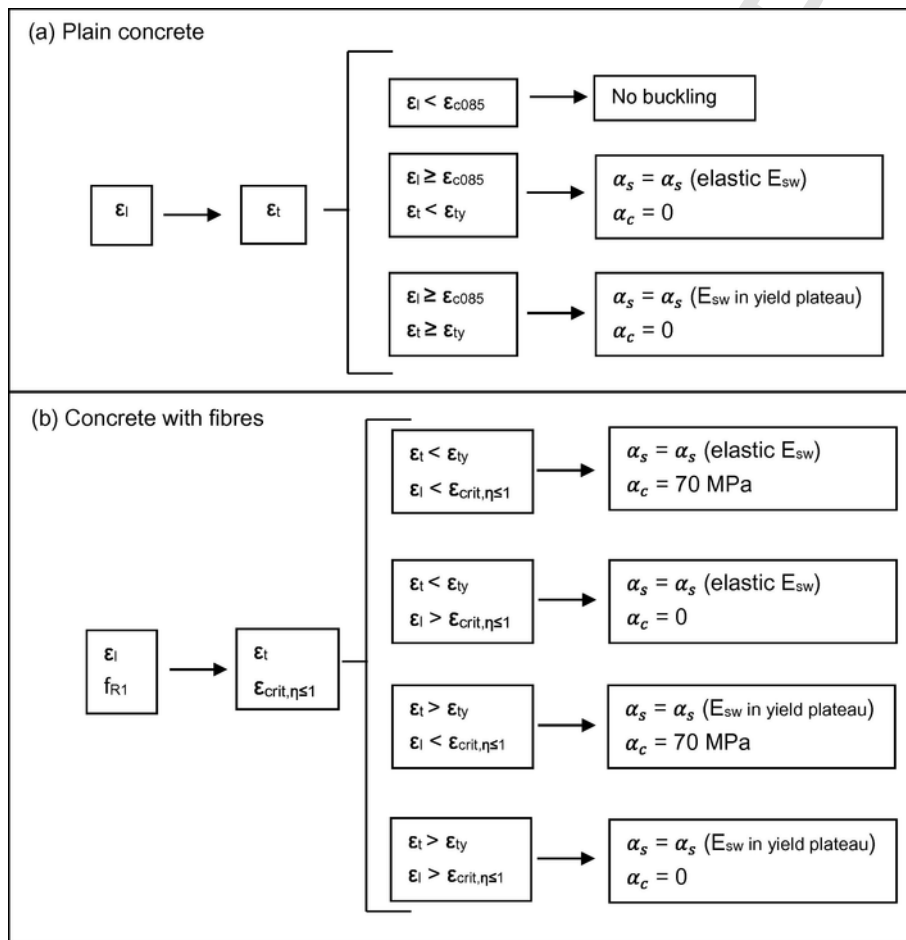
[33,34].

Fig. 16. Scheme from obtaining α_s and α_c.
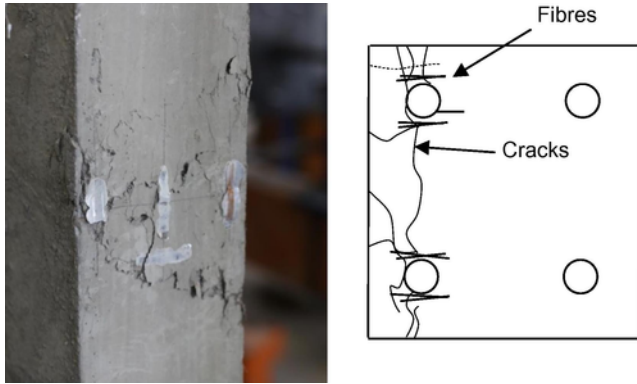
Fig. 17. The concrete cover division in many zones.

References

[1] Fomento EM de, Hormigón ECP del. EHE-08: Instrucción de Hormigón Estructural: con comentarios de los miembros de la Comisión Permanente del Hormigón; 2008.

[2] EN 1998-1; Eurocode 8: Design of structures for earthquake resistance – Part 1: General rules, seismic actions and rules for buildings; 2004.

[3] EN 1998-2; Eurocode 8: Design of concrete structures – Part 2: Bridges; 2005.

[4] ACI Committee 318. ACI 318-14: Building Code Requirements for Structural Concrete and Commentary; 2014.

[5] K.E. Caballero-Morrison, J.L. Bonet, J. Navarro-Gregori, J.R. Martí-Vargas, Behaviour of steel-fibre-reinforced normal-strength concrete slender columns under cyclic loading, Eng Struct 39 (2012) 162–175, http://dx.doi.org/10.1016/j.engstruct.2012.02.003.

[6] K.E. Caballero-Morrison, J.L. Bonet, J. Navarro-Gregori, P. Serna-Ros, An experimental study of steel fiber-reinforced high-strength concrete slender columns under cyclic loading, Eng Struct 57 (2013) 565–577, http://dx.doi.org/10.1016/j.engstruct.2012.06.052.

[7] Paultre P, Eid R, Langlois Y, Lévesque Y. Behavior of steel fiber-reinforced high-strength concrete columns under uniaxial compression read more. ASCE 2010;136 <http://ascelibrary.org/doi/abs/10.1061/%28ASCE%29ST.1943-541X.0000211>.

[8] M. Papia, G. Russo, G. Zingone, Instability of longitudinal bars in RC columns, J Struct Eng 114 (1988) 445–461.

[9] R.P. Dhakal, K. Maekawa, Reinforcement stability and fracture of cover concrete in reinforced concrete members, J Struct Eng 128 (2002) 1253–1262.

[10] R.P. Dhakal, Post-peak response analysis of SFRC columns including spalling and buckling, Struct Eng Mech 22 (2006) 311–330.

[11] G. Campione, Compressive behavior of short fibrous reinforced concrete members with square cross-section, Struct Eng Mech 37 (2011) 649–669.

[12] Mander JB. University of Canterbury. Seismic Design of Bridge Piers; 1983.

[13] J.B. Mander, F.D. Panthaki, A. Kasalanati, Low-cycle fatigue behavior of reinforcing steel, J Mater Civ Eng 6 (1994) 453–468.

[14] G. Monti, C. Nuti, Nonlinear cyclic behavior of reinforcing bars including buckling, J Struct Eng 118 (1992) 3268–3284.

[15] M.E. Rodriguez, J.C. Botero, J. Villa, Cyclic stress-strain behavior of reinforcing steel including effect of buckling, J Struct Eng 125 (1999) 605–612.

[16] O. Bayrak, S.A. Sheikh, Plastic hinge analysis, J Struct Eng 127 (2001) 1092–1100.

[17] S. Bae, A.M. Mieses, O. Bayrak, Inelastic buckling of reinforcing bars, J Struct Eng 131 (2005) 314–321, http://dx.doi.org/10.1061/(ASCE)0733-9445(2005)131:2(314).

[18] Bresler B, Gilbert PH. Tie requirements for reinforced concrete columns. J Proc 1961;58. http://dx.doi.org/10.14359/7997.

[19] Scribner Charles F. Reinforcement buckling in reinforced concrete flexural members. J Proc 1986;83. doi: http://dx.doi.org/10.14359/2648.

[20] Chen Wai-Fah, Lui EM. Structural stability: theory and implementation. PTR Prentice Hall; 1987.

[21] Talaat MM, Mosalam KM. Computational modeling of progressive collapse in reinforced concrete frame structures. ProQuest; 2007.

[22] A. Khajeh, M. Attard, Lateral behaviour of concrete, World Acad Sci Eng Technol 59 (2011) 940–945.

[23] W.P. Lokuge, J.G. Sanjayan, S. Setunge, Stress-strain model for laterally confined concrete, J Mater Civ Eng 17 (2005) 607–616, http://dx.doi.org/10.1061/(ASCE)0899-1561(2005) 17:6(607).

[24] E. Montoya, F.J. Vecchio, S.A. Sheikh, Compression field modeling of confined concrete: constitutive models, J Mater Civ Eng 18 (2006) 510–517, http://dx.doi.org/10.1061/(ASCE)0899-1561(2006) 18:4(510).

[25] E. Osorio, J.M. Bairán, A.R. Marí, Lateral behavior of concrete under uniaxial compressive cyclic loading, Mater Struct (2012) http://dx.doi.org/10.1617/s11527-012-9928-9.

[26] EN 1992-1-1; Eurocode 2: Design of concrete structures – Part 1–1: General rules and rules for buildings; 2004.

[27] Asociación española de normalización y certificación, AENOR. UNE-EN 12390-3. Ensayos de hormigón endurecido – Parte 3: Determinación de la resistencia a compresión de probetas; 2000.

[28] Asociación española de normalización y certificación, AENOR. UNE-EN 14651:2007. Método de ensayo para hormigón con fibras metálicas. Determinación de la resistencia a la tracción por flexión (límite de proporcionalidad (LOP), resistencia residual; 2007.

[29] AENOR. Spanish Association for Standards and Certification. UNE-EN 10002-1. Metallic materials. Tensile testing. Part 1: Method of test at ambient temperature; 2002.

[30] L.L. Dodd, J.I. Restrepo-Posada, Model for predicting cyclic behavior of reinforcing steel, J Struct Eng 121 (1995) 433–445.

[31] G. Campione, M. Fossetti, M. Papia, Behavior of fiber-reinforced concrete columns under axially and eccentrically compressive loads, ACI Struct J 107 (2010) 272–281.

[32] S.J. Pantazopoulou, Detailing for reinforcement stability in RC members, J Struct Eng 124 (1998) 623–632.

[33] E.M. de Fomento, E.C.P. del Hormigón, EHE-08: Instrucción de Hormigón Estructural : con comentarios de los miembros de la Comisión Permanente del Hormigón, Ministerio de Fomento, Secretaría General Técnica, 2008.

[34] ACI Committee. Building Code Requirements for Structural Concrete (ACI 318-08) and Commentary. American Concrete Institute; 2008.